Yamaji, M.; Suwa, Y.; Shimokawa, R.; Paris, C.; Miranda Alonso, MÁ. (2015). Photochemical reactions of halogenated aromatic 1,3-diketones in solution studied by steady state, one- and two-color laser flash photolyses. Photochemical & Photobiological Sciences. 14(9):1673-1684. https://doi.org/10.1039/c5pp00211g

The Electronic Supplementary Information for

Photochemical reactions of halogenated aromatic 1,3-diketones in solution studied by steady state, one- and two-color laser flash photolyses

Minoru Yamaji,[a,*] Yurie Suwa,[b] Rieko Shimokawa,[b] Cecilia Paris[c] and Miguel Ángel Miranda[c,*]

[a] *Division of Molecular Science, Graduate School of Science and Technology, Gunma University, Kiryu, Gunma 376-8515, Japan*
[b] *Education Program of Materials and Bioscience, Graduate School of Science and Engineering, Gunma University, Kiryu, Gunma 376-8515, Japan*
[c] *Instituto de Tecnologia Química UPV-CSIC, Universidad Politécnica de Valencia, Valencia, Spain*

Contents

1. Preparation and NMR data for BrPB@Ph, ClPB@Ph, PB@F, PB@T, BrPB@F, BrPB@T, ClPB@F and ClPB@T

1-1. Preparation of BrPB@Ph

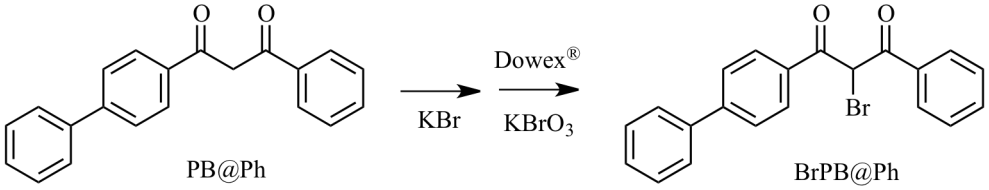

1-Biphenyl-4-yl-3-phenyl-propane-1,3-dione (PB@Ph, 210 mg, 0.7 mmol), KBr (83.3 mg, 0.7 mmol), Dowex® 1.4 g were added to MeOH (10 ml), and the solution was stirred at 0 °C for 10 min. After adding $KBrO_3$ (117 mg, 0.7 mmol), the solution was stirred at 0 °C for 30 min. The products were extracted with benzene (100 ml), the solution was washed with brine, dried with Na_2SO_4, and evaporated in vacuum. The product was separated using silica gel column chromatography with hexane/ethyl acetate (3:1, v/v) as the eluent, showing a spot on TLC at Rf = 0.37, providing 130 mg BrPB@Ph. Yield 49 %. ^{1}H NMR ($CDCl_3$, 400 MHz) δ_H 8.06 (d, 2H, J = 8.70), 8.00 (d, 2H, J = 7.10), 7.68 (d, 2H, J = 8.70), 7.60 (d, 2H, J = 8.24), 7.51-7.40 (m, 6H), 6.56 (s, 1H). The obtained NMR data are consistent with those in the literature.[1]

1.2 Preparation of ClPB@Ph

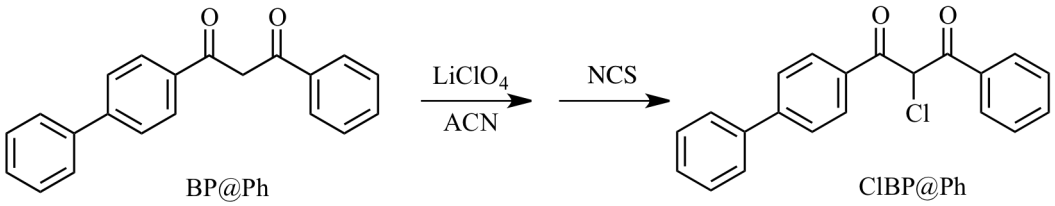

PB@Ph (600 mg, 2 mmol) and $LiClO_4$ (130 mg, 1.22 mmol) were added to acetonitrile (25 ml), and the solution was stirred at room temperature for 10 min. After adding *N*-chlorosuccinimide (NCS, 294 mg, 2.2 mmol), the solution was stirred at room temperature for 3 h. After the solvent was evaporated, benzene (100 ml) was added. The solution was washed with brine, dried with Na_2SO_4, and evaporated in vacuum. The product was separated using silica gel column chromatography with hexane/ethyl acetate (9:1, v/v) as the eluent, showing a spot on TLC at Rf = 0.17. Recrystallization from hexane provided purified 430 mg ClPB@Ph. Yield 64 %. ^{1}H NMR ($CDCl_3$, 400 MHz) δ_H 8.07 (d, 2H, J = 8.70), 8.01 (d, 2H, J = 7.33), 7.68 (d, 2H, J = 8.47), 7.59 (d, 2H, J = 7.79), 7.51-7.37 (m, 6H), 6.42 (s, 1H).

1.3 Preparation of PB@F

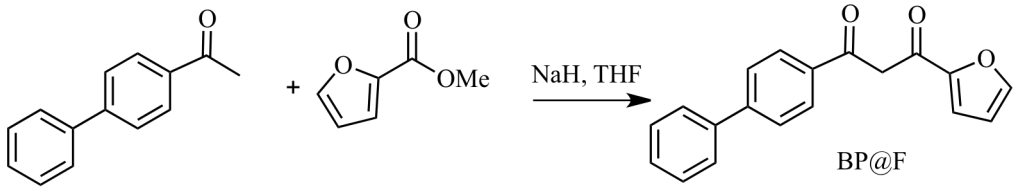

To suspended NaH (600 mg) in dry THF (5 ml), 4-acetylbiphenyl (294 mg, 1.5 mmol) was added, and the solution was stirred for 3 min. The solution added with methyl 2-furorate (0.21 ml, 1.65 mmol) was refluxed for 24 h, and aqueous NH_4Cl was added. The product was extracted with ethyl acetate, washed with brine, and the solvent was evaporated in vacuum. The product was separated using silica-gel column chromatography with hexane/ethyl acetate (9:1, v/v) as the eluent, showing a spot on TLC at Rf = 0.29, providing 150 mg PB@F. Yield 34 %. ^{1}H NMR ($CDCl_3$, 400 MHz) δ_H 8.03 (d, 2H, J = 8.70), 7.70 (d, 2H, J = 8.47), 7.65-7.59 (m, 3H), 7.51-7.37 (m, 3H), 7.26 (d, 2H, J = 3.43), 6.80 (s, 1H), 6.59 (dd, 1H, J = 1.83, 3.43).

1.4 preparation of PB@T

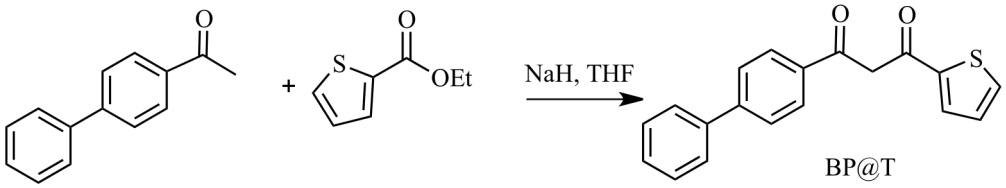

To suspended NaH (600 mg) in dry THF (5 ml), 4-acetylbiphenyl (294 mg, 1.5 mmol) was added, and the solution was stirred for 3 min. The solution added with methyl thiophene-2-carboxylic acid ethyl ester (0.26 ml, 1.65 mmol) was refluxed for 24 h, and aqueous NH_4Cl was added. The product was extracted with ethyl acetate, washed with brine, and the solvent was evaporated in vacuum. The product was separated using silica gel column chromatography with hexane/ethyl acetate (9:1, v/v) as the eluent, showing a spot on TLC at Rf = 0.32, providing 350 mg PB@T. Yield 76 %. ^{1}H NMR ($CDCl_3$, 400 MHz) δ_H 8.02 (d, 2H, J = 8.47), 7.82 (d, 1H, J = 3.66), 7.70 (d, 2H, J = 8.47), 7.66-7.61 (m, 3H), 7.51-7.38 (m, 4H), 7.18 (dd, 1H, J = 3.89, 4.81), 6.72 (s, 1H).

1-5. Preparation of BrPB@F

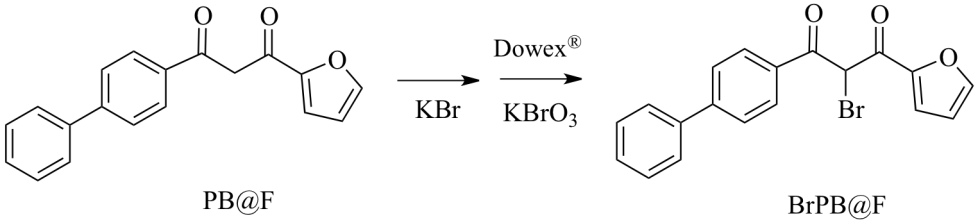

1-Biphenyl-4-yl-3-furan-2-yl-propane-1,3-dione (PB@F, 290 mg, 1 mmol), KBr (119 mg, 1 mmol) and Dowex® (2 g) were added to methanol (15 ml), and the solution was stirred at 0 °C

for10 min. After adding $KBrO_3$ (167 mg, 1 mmol), the solution was stirred at 0 °C for 30 min. The products were extracted with benzene (100 ml), the solution was washed with brine, dried with Na_2SO_4, and evaporated in vacuum. The product was separated using silica gel column chromatography with hexane/ethyl acetate (3:1, v/v) as the eluent, showing a spot on TLC at Rf = 0.28, providing 230 mg BrPB@F. Yield 62 %. ^{1}H NMR ($CDCl_3$, 400 MHz) δ_H 8.09 (d, 2H, J = 8.70), 7.70 (d, 2H, J = 8.70), 7.62-7.59 (m, 3H), 7.51-7.39 (m, 4H), 6.58 (dd, 1H, J = 1.83, 3.66), 6.41 (s, 1H). The obtained data are consistent with those in the literature.[1]

1-6. Preparation of BrPB@T

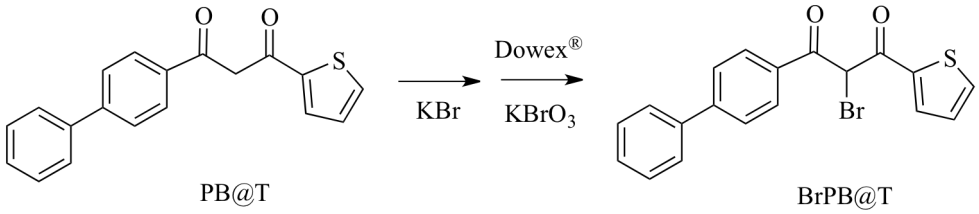

1-Biphenyl-4-yl-3-thiophen-2-yl-propane-1,3-dione (PB@T, 306 mg, 1 mmol), KBr (119 mg, 1 mmol) and Dowex® (2 g) were added to methanol (15 ml), and the solution was stirred at 0 °C for 10 min. After adding $KBrO_3$ (167 mg, 1 mmol), the solution was stirred at 0 °C for 30 min. The products were extracted with benzene (100 ml), the solution was washed with brine, dried with Na_2SO_4, and evaporated in vacuum. The product was separated using silica gel column chromatography with hexane/ethyl acetate (3:1, v/v) as the eluent, providing 160 mg BrPB@T. Yield 42 %. ^{1}H NMR ($CDCl_3$, 400 MHz) δ_H 8.10 (d, 2H, J = 8.47), 7.87 (dd, 1H, J = 1.14, 3.89), 7.72-7.67 (m, 3H), 7.60 (d, 2H, J = 6.89), 7.51-7.37 (m, 3H), 7.13 (dd, 1H, J = 3.89, 5.04), 6.34 (s, 1H).

1-7. Preparation of ClPB@F

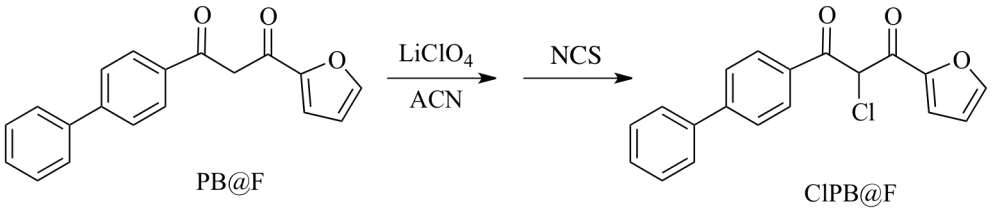

1-Biphenyl-4-yl-3-furan-2-yl-propane-1,3-dione (PB@F, 435 mg, 1.5 mmol) and $LiClO_4$ (98 mg, 0.9 mmol) were added to acetonitrile (20 ml), and the solution was stirred at room temperature for 10 min. After adding NCS (221 mg, 1.7 mmol), the solution was stirred at room temperature for 4 h. After the solvent was evaporated, benzene (100 ml) was added. The solution was washed with brine, dried with Na_2SO_4, and evaporated in vacuum. The product was separated using silica-gel column chromatography with hexane/ethyl acetate (3:1, v/v) as the eluent, showing a spot on TLC at Rf = 0.29, providing 270 mg ClPB@F. Yield 55 %. ^{1}H NMR ($CDCl_3$, 400 MHz)

δ_H 8.10 (d, 2H, J = 8.5), 7.70 (d, 2H, J = 8.5), 7.62-7.58 (m, 3H), 7.51-7.39 (m, 4H), 6.58 (dd, 1H, J = 1.6, 3.7), 6.28 (s, 1H).

1-8. Preparation of ClPB@T

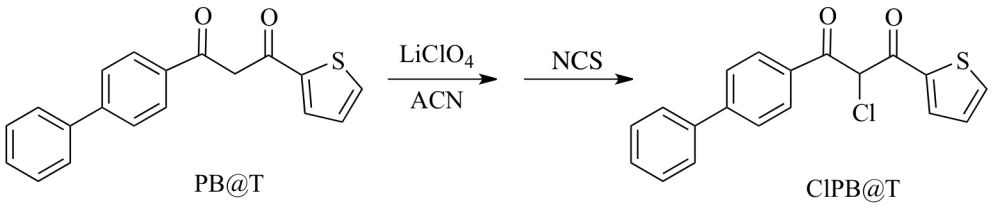

PB@T ClPB@T

1-Biphenyl-4-yl-3-thiophen-2-yl-propane-1,3-dione (PB@T, 306 mg, 1.0 mmol) and $LiClO_4$ (65 mg, 0.61 mmol) were added to acetonitrile (20 ml), and the solution was stirred at room temperature for 10 min. After adding *N*-chlorosuccinimide (NCS, 65 mg, 0.6 mmol), the solution was stirred at room temperature for 4 h. After the solvent was evaporated, benzene (100 ml) was added. The solution was washed with brine, dried with Na_2SO_4, and evaporated in vacuum. The product was separated using silica gel column chromatography with hexane/ethyl acetate (3:1, v/v) as the eluent, showing a spot on TLC at Rf = 0.43, providing 341 mg ClPB@T. Yield 44 %. ^{1}H NMR ($CDCl_3$, 400 MHz) δ_H 8.11 (d, 2H, J = 8.47), 7.92 (d, 1H, J = 3.89), 7.72 (d, 1H, J = 4.81), 7.68 (d, 2H, J = 8.47), 7.60 (d, 2H, J = 7.56), 7.48-7.38 (m, 3H), 7.14 (dd, 1H, J = 4.12, 4.81), 6.22 (s, 1H).

2. Absorption and emission spectra of PB@F, PB@T and the halogenated diketones

Figure S1 shows absorption and emission spectra of PB@F, PB@T and the halogenated compounds in solution. From the wavelength regions of the absorption maxima, the molecular configurations of these compounds are inferred. PB@F and PB@T are in the enol form while the other halogenated diketones are in the keto form.

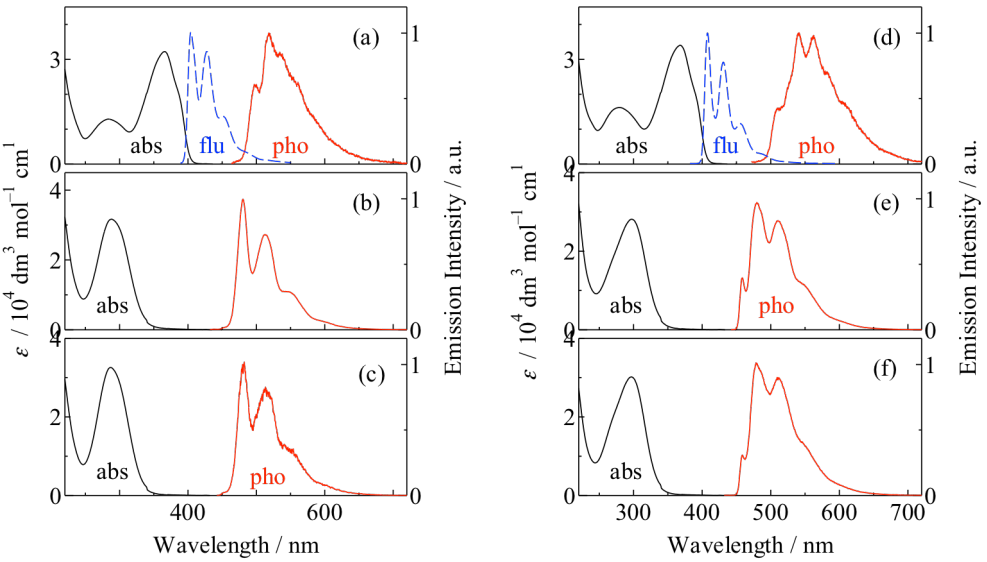

Figure S1. Absorption spectra (solid) in ACN at 295 K and phosphorescence spectra (red) in EtOH at 77 K for PB@F (a), BrPB@F (b), ClPB@F (c), PB@T (d), BrPB@T (e) and ClPB@T (f). Fluorescence (blue) was observed for PB@F (a) and PB@T (d) in EtOH at 77 K whereas that from BrPB@F, ClPB@F, BrPB@T and ClPB@T was not observed at 295 K and 77 K.

3. Photochemical features studied by absorption spectrum measurements

3.1 Absorption spectrum measurements of BrPB@F and BrPB@T upon stationary photolysis

Figures S2 and 3 show absorption spectral changes upon photolysis of BrPB@F and BrPB@T in EtOH and CH, respectively. Absorption spectrum of BrPB@F in EtOH consists of that for the keto form at 280 nm and probably that for the enol form of BrPB@F at 378 nm (Figure S2a). BrPB@F showed absorption spectral changes without isosbestic points upon photolysis in EtOH, providing an absorption band at 360 nm due to PB@F. Consequently, photolysis of BrPB@F in EtOH provides PB@F via debromination in the S_1 state. Conversely, BrPB@T decomposed and gave rise to the absorption band of PB@T with isosbestic points (Figure S2b). The fact of forming PB@T demonstrates occurrence of photodebromination from BrPB@T in EtOH. The quantum yield for the PB@T formation was determined to be 0.10 ± 0.01, which was independent of the amount of the dissolved oxygen. The photodebromination of BrPB@T in EtOH also proceeds in the S_1 state.

In CH, as increasing the irradiation time, BrPB@F and BrPB@T decompose with isosbestic points, providing absorption shoulders at 350 nm, which are different from the absorption bands of the corresponding dehalogenated compounds (Figure S3). We were unable to identify the photoproducts due to the absorption shoulders at 350 nm from the final absorption spectra.

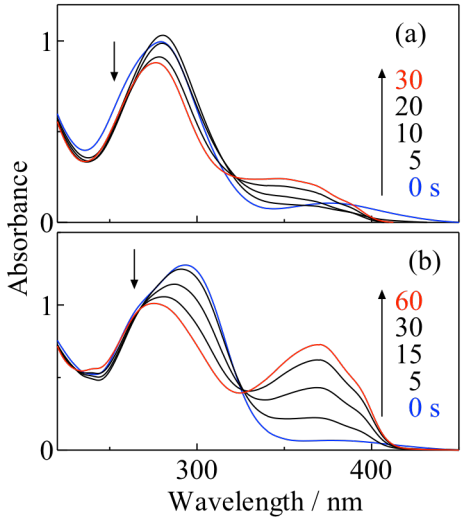

Figure. S2 Absorption spectral changes upon photolysis (λ＞280 nm) of BrPB@F and BrPB@T in EtOH.

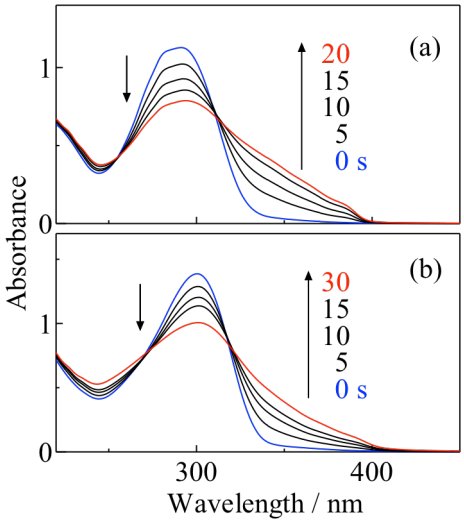

Figure. S3 Absorption spectral changes upon photolysis (λ＞280 nm) of BrPB@F and BrPB@T in CH.

3.2 Photolysis of *p*-methoxyphenacyl chloride and *p*-*tert*-butylbenzaldehyde in aerated ACN

Figure S4 shows absorption spectral changes upon 254 nm photolysis of *p*-methoxyphenacyl chloride in aerated ACN. As increasing the irradiation time, the absorbance at 275 nm decreased, giving an absorption spectrum having the maximum at 220 nm at 300 s (PP_{220}). On the other hand, photolysis of *p*-*tert*-butylbenzaldehyde in aerated ACN gave no changes in the absorption spectrum.

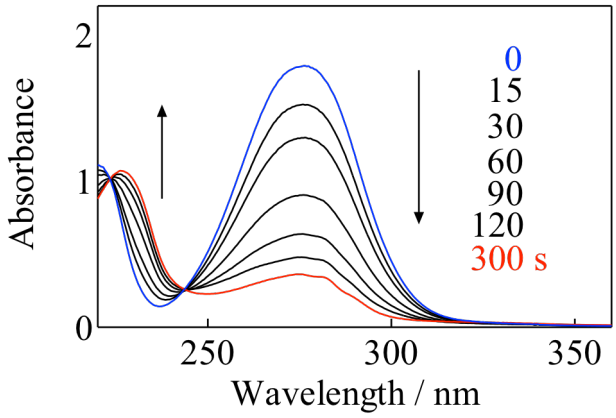

Figure S4. Absorption spectral changes upon 254 nm photolysis of *p*-methoxyphenacyl chloride in aerated ACN.

3.3 Photolysis of *p*-phenylphenacyl chloride and benzaldehyde in aerated ACN

Figure S5 shows absorption spectral changes upon 254 nm photolysis of ClPB@Ph and *p*-phenylphenacyl chloride in aerated CH and the reference spectra of PP_{276} and benzaldehyde. As increasing the irradiation time, the absorbance at 295 nm of ClPB@Ph decreased, giving an absorption spectrum having the maximum at 276 nm at 360 s (PP_{276}). On the other hand,

photolysis of *p-tert*-butylbenzaldehyde in aerated ACN gave no changes in the absorption spectrum (λ_{max} = 243 nm; ε_{243} = 14900 dm^3 mol^{-1} cm^{-1} in CH).

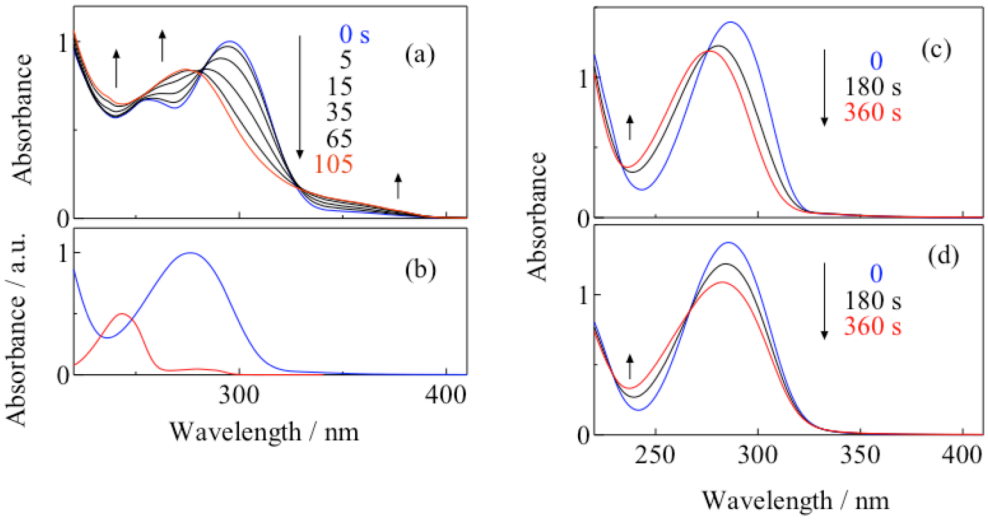

Figure S5. (a) Absorption spectral changes upon photolysis (λ > 280 nm) of ClPB@Ph in aerated CH. (b) Reference absorption spectra of PP_{276} (blue) and benzaldehyde (red). (c) Absorption spectral changes upon photolysis (λ > 280 nm) of *p*-phenylphenacyl chloride in aerated CH. (d) Absorption spectral changes upon photolysis (λ > 280 nm) of *p*-phenylphenacyl chloride in aerated CH.

3.4 Absorption spectral changes upon steady state photolysis of ClPB@Ph in ACN and the absorption spectra of the isolated photoproducts

Figure S6a shows absorption spectral changes upon photolysis of ClPB@Ph in ACN, which have been shown as Figure 4b in the text. We were succeeded in isolating the photoproducts (PP_{253} and PP_{283}) having the absorption peaks at 253 nm and 283 nm using a home-made microflow photoreactor. The absorption spectra of PP_{253} and PP_{283} are shown as Figure S6b and c, respectively. Superposing these absorption spectra well reproduced the absorption spectra at 105 s in Figure S6a.

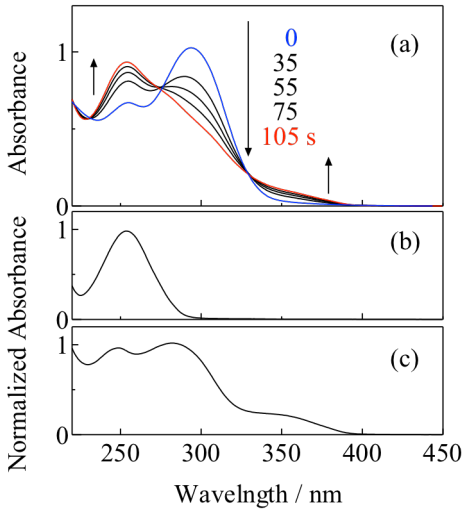

Figure S6. (a) Absorption spectral changes upon photolysis (λ>270 nm) of ClPB@Ph in aerated ACN. Reference absorption spectra of PP_{253} (b) and PP_{283} (c) in ACN.

3.5 Absorption measurements of ClPB@F and ClPB@T upon stationary photolysis

Figure S7 shows absorption spectral changes upon photolysis of ClPB@F. In CH, as increasing the irradiation time, the absorbance of ClPB@F at 290 nm decreased whereas an absorption band at 366 nm due to PB@F appeared (Figure S7a). These absorption changes indicate occurrence of dechlorination from ClPB@F, followed by H-atom abstraction from CH by the produced dechlorinated radical. In ACN, isosbestic poins appear on photodecomposition of ClPB@F, giving a broad absorption band in the wavelength region, 320 - 400 nm consisted not only of the charactristic absorption band (λ_{max} = 366 nm) of PB@F (Figure S7b). α-Bond dissociation might be a concomitant reaction. In EtOH the absorption band for the enol form of ClPB@F is observed before photorradiation as well as seen for BrClPB@F in EtOH (Figure S2a), but after starting photolysis, absorption changes similar to those in ACN were seen (Figure S7c). We were unable to analyze photochemical reactions of ClPB@F in EtOH. The observed photochemical reactions in these solvents proceeded irrespective of the presence of the dissolved oxygen. Thus, the photodecomposition of ClPB@F is the event in th S_1 state.

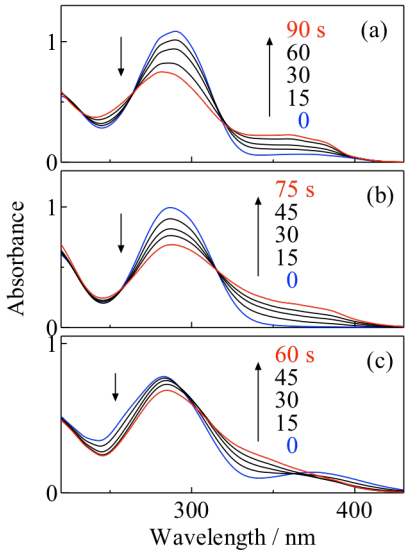

Figure S7. Absorption spectral changes upon photolysis (λ＞270 nm) of ClPB@F in CH (a), ACN (b) and EtOH (c).

Figure S8 shows absorption spectral changes upon photolysis of ClPB@T in CH and ACN. In both the solvents, the absorption band of ClPB@T diminished with isosbestic points, giving rise to the absorption band due to PB@T at 360 nm independent of the amount of the dissolved oxygen. These absorption spectral changes indicate the dechlorination of ClPB@F in the S_1 state.

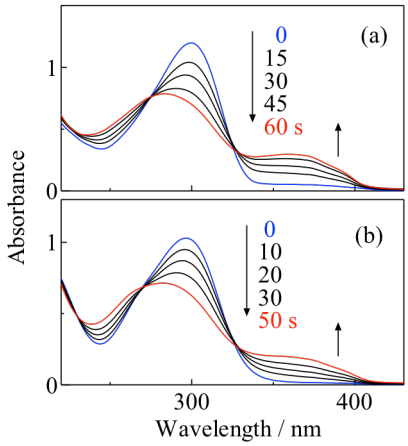

Figure S8. Absorption spectral changes upon photolysis (λ＞270 nm) of ClPB@T in CH (a) and ACN (b).

4. Determining Φ_{AB} by using laser photolysis techniques

Figure S9 shows absorbance changes, ΔA_λ due to the formed species (λ = 356 nm for AB and λ = 343 nm for MC) obtained upon 266 nm laser photolysis of BrAB in EtOH and MDPA in MCH plotted as a function of the term, $1\text{-}10^{-A_{266}}$. The Plots show straight lines. From the slope to the lines and eqns 1 and 2, the value of Φ_{AB} in EtOH was determined to be 0.07 ± 0.01.

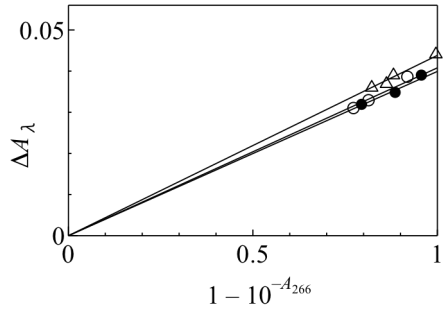

Figure S9. Absorbance changes, ΔA_λ at λ nm obtained upon 266 nm laser photolysis of BrAB in degassed EtOH (○; λ = 356 nm) and aerated EtOH (●; λ = 356 nm), and of MDPA in aerated MCH (△; λ = 343 nm) plotted as a function of the term, $1\text{-}10^{-A_{266}}$.

5. Transient absorption measurements by 308 nm laser flash photolysis

5.1 Laser flash photolysis of BrPB@F and BrPB@T

Figure S10 shows transient absorption spectra of BrPB@F and BrPB@T upon 308 nm laser pulsing in EtOH. Absorption bands at 450 nm for BrPB@F and BrPB@T seen at 80 ns diminished with a decay lifetime of 4.9 μs, which was shortened in the presence of the dissolved oxygen. The observed absorption bands at 450 nn are ascribable to the T-T absorption of BrPB@F and BrPB@T. As increasing the time, absorption bands at 355 nm for ClPB@F and 265 nm for ClPB@T, which are consistent with those of PB@F and PB@T, respectively, appeared in the millisecond time domain. The increasing features of the bands were independent of the presence of the dissolved oxygen. From these observations of the transient data, debromination and intersystem crossing to the T_1 state are concomitants in the S_1 states of BrPB@F and BrPB@T in EtOH.

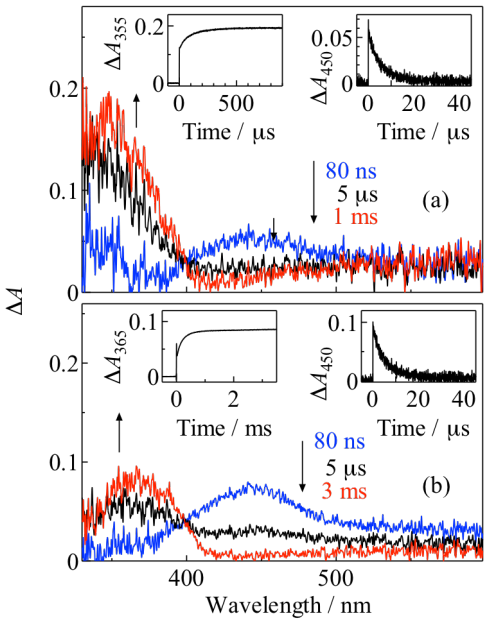

Figure S10. Transient absorption spectra obtained upon 308 nm laser pulsing in degassed EtOH solution of BrPB@F (a) and BrPB@T (b). Insets; temporal absorbance at 355 nm (upper, left), 450 nm (upper, right), 365 nm (lower, left) and 450 nm (lower, right).

Figure S11 shows transient absorption spectra of BrPB@F and BrPB@T upon 308 nm laser in CH. At 80 ns after laser pulsing in the CH solution, transient absorption bands at 500 nm for ClPB@F and 453 nm for BrPB@T were observed. The absorbance of these bands decreased with lifetimes of 7.2 μs for BrPB@F and 5.8 μs for BrPB@T. These lifetimes were independent of the presence of the dissolved oxygen. These transient absorption bands are, therefore, not for the triplet manifolds. In the tens microsecond time domain, absorption bands at 337 nm for ClPB@F and 340 nm for BrPB@T appeared. Absorption maxima of these bands are different from those of the corresponding nonhalogenated enol forms. We have not observed the debromination from these compounds in CH by steady state photolysis studies. We were unable to identify the chemical reactions of these compounds in CH from the transient absorption measurements. We can say that the photochemical reactions of BrPB@F and BrPB@T strictly depend on the variety of the solvent.

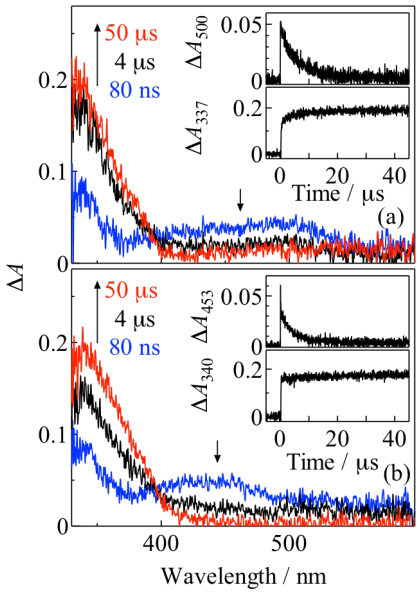

Figure S11. Transient absorption spectra upon 308 nm laser pulsing in degassed CH solution of BrPB@F (a) and BrPB@T (b). Insets; temporal absorbance at 500 nm (upper in (a)), 337 nm (lower in (b)), 453 nm (upper in (b)) and 340 nm (lower in (b)).

5.2 Laser flash photolysis of ClPB@F and ClPB@T

Figures S12 and 13, respectively, show transient absorption spectra of ClPB@F and ClPB@T at 80 ns upon 308 nm laser pulsing. Transient absorption spectra located in the wavelength region, 440 - 460 nm have the similar spectral features. The lifetimes of the absorption bands for ClPB@F were 100 ns in CH, 80 ns in ACN and 140 ns in EtOH whereas those for ClPB@T were 260 ns in CH and 90 ns in ACN. Since the lifetimes were shortened in the presence of the dissolved oxygen, the observed transient absorption spectra are due to the triplet states of the corresponding chlorinated diketones. We have recognized that these chlorinated diketones mainly undergo photodechlorination in the S_1 state. Observation of the triplet state indicates that intersystem crossing from the S_1 to the T_1 is efficient in these chlorinated diketones. After depletion of the T-T absorption, no residual absorption was found in the wavelength region longer than 400 nm.

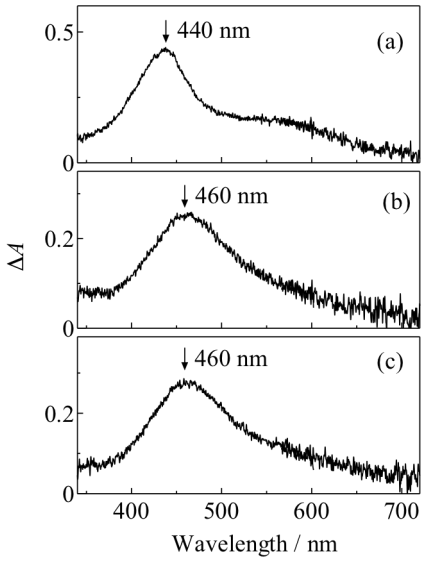

Figure S12. Transient absorption spectra obtained at 80 ns upon 308 nm laser pulsing of ClPB@F in degassed CH (a), ACN (b) and EtOH (c).

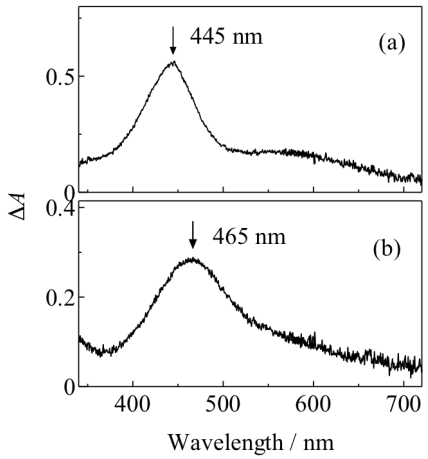

Figure S13. Transient absorption spectra at 80 ns upon 308 nm laser pulsing of ClPB@T in degassed CH (a) and ACN (b).

6. Dechlorination in a higher triplet state studied by two-color two-laser photolysis

We have obtained relatively intense T-T absorption of ClPB@F and ClPB@T in CH upon 308 nm laser photolysis, two-color two-laser photolysis of these compound in CH was performed. The wavelength of the second laser pulse was adopted 440 nm. The first excitation with a 308 nm laser pulse produces the triplet absorption that efficiently absorbs the second 440 nm laser pulse with a 50 ns delay. The 440 nm laser pulse is, thus, absorbed only by the triplet. Figures S14 and 15 show absorption spectral changes upon one and two-laser pulsing of ClPB@F and ClPB@T, respectively in CH. As increasing the number of one-color laser pulses, absorption due to the dechlorinated diketones appears at 360 nm. In the presence of the second 440 nm laser pulse, more intense absorption at 360nm can be recognized in Figure S14b and 15b. In order to make clear the difference in the absorbance, subtraction between the absorption spectra obtained by one and two-color laser pulsing was executed (Figures S14c and 15c). The obtained difference spectra, which agree with those of the nonchlorinated diketones, are originated from the dechlorination upon exciting the T_1 states. These results convince that dechlorination unambiguously proceeds in a higher triplet (T_n) state. The quantum yields for dechlorination in the T_n state were too small to determine by laser photolysis techniques.

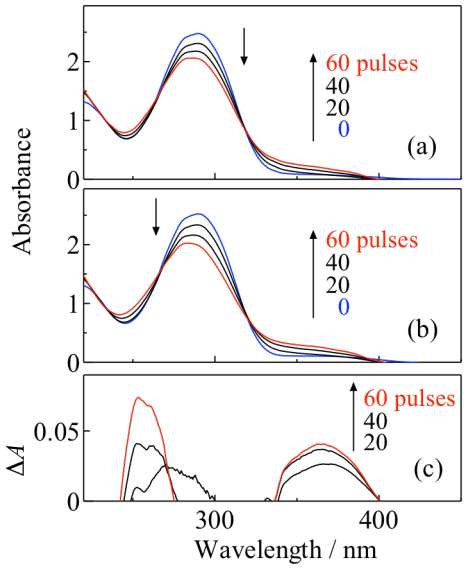

Figure S14. Absorption spectral changes after 308 nm laser pulsing (a) and 308 nm plus 50 ns delayed 440 nm laser pulsing (b) in the degassed CH of ClPB@F. (c) Difference absorption spectra between ones in (a) and (b) at the corresponding number of the laser pulses.

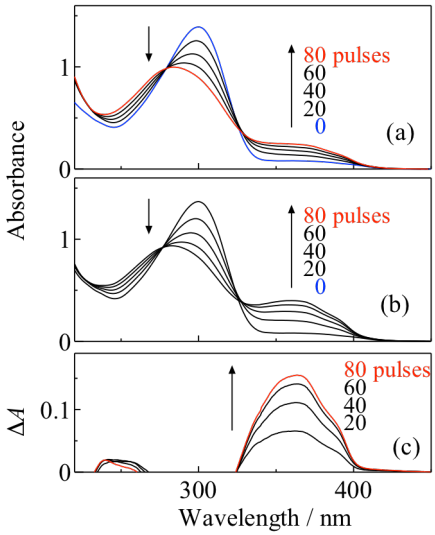

Figure S15. Absorption spectral changes after 308 nm laser pulsing (a) and 308 nm plus 50 ns delayed 440 nm laser pulsing (b) in the degassed CH of ClPB@T. (c) Difference absorption spectra between ones in (a) and (b) at the corresponding number of the laser pulses.

7. DFT calculation for Heat of formation and the schematic configurations of the radicals

The calculation was carried out at the DFT level, using the Gaussian 09 software package. The geometries of XDK and DKR were fully optimized by using the 6-31G(d) base set at the UB3LYP method. 1 Hartree = 627.5095 kcal mol^{-1}.

Table S1. Calculated heats of formation for XDK.

XDK	$\Delta_f H$ (XDK) / hartree
BrAB	-3571.759521
ClAB	-1460.245691
BrPB@Ph	-3531.104577
ClPB@Ph	-1419.590798
BrPB@F	-3528.912714
ClPB@F	-1417.399767
BrPB@T	-3851.896107
ClPB@T	-1740.380837

Table S2. Calculated heats of formation for the radicals produced by dehalogenation.

Radical	$\Delta_f H$(X) / hartree	$\Delta_f H$(DKR) / hartree
Br	-2571.654558	-
Cl	-460.133882	-
ABR	-	-1000.013437
PB@PhR	-	-959.356676
PB@FR	-	-957.162304
PB@TR	-	-1280.14775

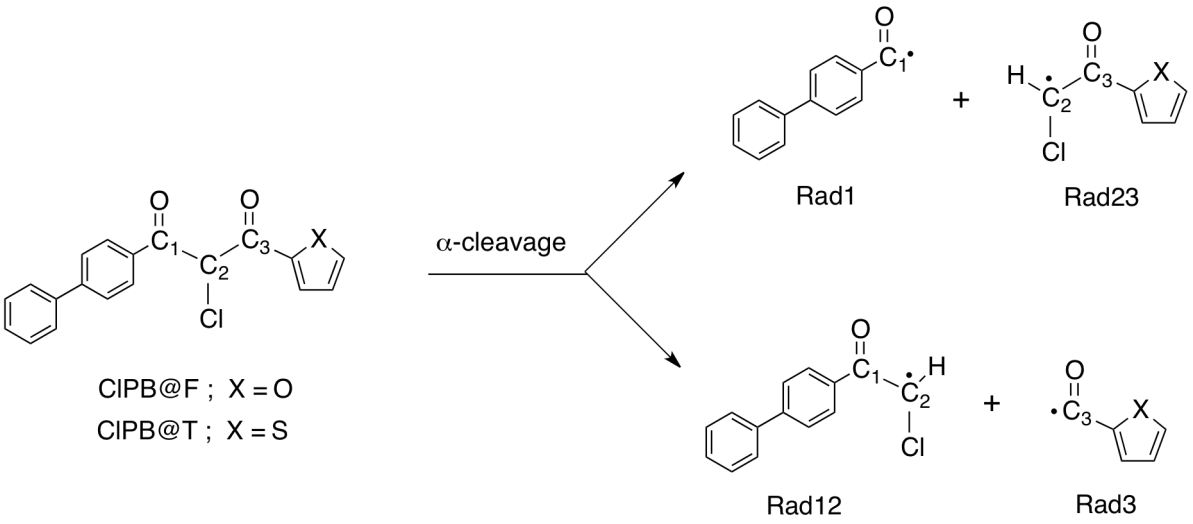

Scheme S1. Possible pathways for of α-cleavage in ClPB@F and ClPB@T with numbered carbon atoms.

Table S3. Calculated heats of formation for the radicals produced by α-cleavage.

ClDK	$\Delta_f H$(Rad1) / hartree	$\Delta_f H$(Rad23) / hartree	$\Delta_f H$(Rad12) / hartree	$\Delta_f H$(Rad3) / hartree
ClAB	-501.952884	-958.194274	-1000.842114	-459.305718
ClPB@Ph	-575.78773	-843.707749	-843.707749	-344.815564
ClPB@F	↑	-841.513097	↑	-342.621252
ClPB@T	↑	-1164.496754	↑	-665.496868

Note and Reference

1. L. Cao, J. Ding, G. Yin, M. Gao, Y. Li and A. Wu, Thioglycoluril as a novel organocatalyst: rapid and efficient α-monobromination of 1,3-dicarbonyl compounds, *Synlett*, 2009, 1445-1448.